# Wafer bonded distributed feedback laser with sidewall modulated Bragg gratings

Olesya Bondarenko,[a] Qing Gu, Janelle Shane, Aleksandar Simic, Boris Slutsky, and Yeshaiahu Fainman
*Department of Electrical and Computer Engineering, University of California San Diego, La Jolla, California 92093-0407, USA*

(Received 18 March 2013; accepted 3 July 2013; published online 23 July 2013)

We demonstrate an optically pumped hybrid III-V/Si distributed feedback laser with a small footprint, using sidewall modulated Bragg gratings for optical feedback. Our approach provides high overlap between lasing mode and gain medium and may enable hybrid lasers with improved efficiency, reduced threshold, and minimal size. We fabricate the structure using plasma-assisted wafer bonding, followed by self-aligned lithography and etching. The latter allows us to avoid alignment errors. This approach is a promising avenue toward ultracompact, energy efficient, and scalable monolithically integrated photonic circuits. © *2013 AIP Publishing LLC*.
[http://dx.doi.org/10.1063/1.4816331]

Modern communication systems place rapidly growing requirements on information processing speed, as well as on the manufacturing and operation cost of their components and networks. One way to meet these needs is to supplement electronic circuits with photonic integrated circuits (PICs). Currently, silicon serves not only as a foundation for CMOS technology, but also as a primary material for passive photonics, due to its numerous advantages for on-chip light transport. However, enabling the full range of functionalities (e.g., switching, routing, lasing, modulation, and detection) on a single module requires the use of other materials.[1–3] In particular, III-V compound semiconductors are advantageous for construction of active optical elements and logic devices, owing to their direct, widely ranging energy bandgap and high carrier mobility.

Today most photonic circuits with active components are implemented via flip-chip bonding of independently fabricated active components to a silicon-based passive photonic circuit. This approach is complex, time consuming, and has tight alignment tolerances (<0.5 μm) for a minimal (≈1 dB per link) coupling loss for microscale components;[4–7] for nanoscale components, the alignment restriction becomes impractical. An alternative way to integrate dissimilar material systems is their monolithic integration through epitaxial growth or wafer bonding prior to the PIC nanofabrication. Despite the remarkable progress with growing epitaxial III-V semiconductor layers on silicon,[8–10] the dissimilar crystal structures of these materials make it extremely challenging to grow sufficiently large areas of III-V on Si for PIC manufacturing.[11] This makes a second alternative approach, wafer bonding, the most amenable for dense, large-scale monolithic integration at present.

Compared to a number of existing wafer bonding techniques,[12] plasma assisted wafer bonding[13] has advantages of scalability, low temperature, and directness. Furthermore, it has already been successfully used to demonstrate a variety of SOI-compatible evanescent optoelectronic devices.[14] We combine plasma-assisted wafer bonding with a self-aligned fabrication approach,[15] which requires a single resist mask to etch both III-V and silicon layers and offers the benefit of simple, alignment-free fabrication. The latter is very important when device dimensions approach the alignment resolution limit of commercial mask aligners.

In this work, we use self aligned sidewall modulated Bragg gratings[16] for optical feedback in a compact III-V/Si distributed feedback (DFB) laser (Figures 1(a) and 1(c)). High mode confinement factor in the gain layer of submicron cross-section waveguide is a potential way to reduce the threshold and enable lasing in hybrid III-V/Si lasers.[17–19] We show the high degree of compactness enabled by our design and fabrication approach by demonstrating lasing in a 100 μm long optically pumped wafer bonded DFB laser.

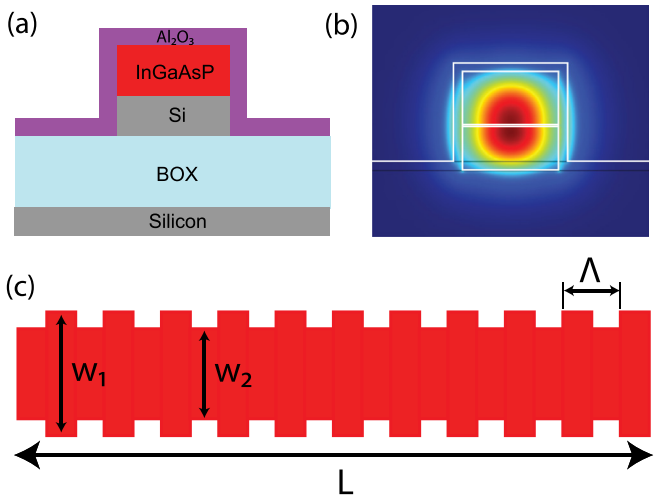


FIG. 1. III-V/Si hybrid DFB laser design: schematic drawing of a III-V/Si DFB laser resonator with vertical sidewall modulated Bragg gratings—cross-section (a) and top view (c); (b) finite element simulation (COMSOL) of a fundamental TE-like mode for a 500 nm wide and 550 nm tall III-V/Si waveguide with 250 nm silicon layer, 300 nm InGaAsP MQW layer, and 50 nm $Al_2O_3$ cladding.

[a]Email: obondarenko@eng.ucsd.edu

 

A schematic drawing of the designed optically pumped laser structure is presented in Figures 1(a) and 1(c). The TE-like transverse optical mode of the composite waveguide is evenly distributed between the silicon and III-V layers (Figure 1(b)). By choosing the III-V/Si layer thickness ratio, we can control the gain-mode overlap, thus providing more effective interaction of the mode with the gain material. With the ability to produce high gain-mode overlap, stimulated emission can be reached either at reduced threshold or with smaller device footprints, depending on the design.

We use coupled mode theory[20] to estimate locations of the stop band of the grating and its adjacent minima, where the lasing is likely to occur. Here we neglect the gain coefficient of the III-V layer and assume a passive Bragg grating with effective indices extracted from cross-sectional finite element simulations in COMSOL (Figure 1(b)). This simple model is sufficient for initial estimation of the grating behavior. The reflectivity of a passive Bragg grating can be expressed as follows:[21]

$$R = \frac{\kappa^* \kappa \sinh^2 sL}{s^2 \cosh^2 sL + (\Delta\beta/2)^2 \sinh^2 sL}, \quad (1)$$

where $s = \sqrt{|\kappa|^2 - (\Delta\beta/2)^2}$, $L$ is the grating length, and $\Delta\beta$ is the detuning of the propagation constant from the stop band center (Bragg wavelength). The coupling coefficient $\kappa$ for the fundamental TE mode of an unperturbed waveguide is defined by

$$\kappa = \frac{\pi}{2\lambda_0} c \int \mathbf{E}_1{}^* \Delta\varepsilon \mathbf{E}_2 dxdy. \quad (2)$$

The electric fields $\mathbf{E}_1$ and $\mathbf{E}_2$, as well as the first order dielectric perturbation tensor $\Delta\varepsilon$, were extracted from COMSOL simulations. We calculate the $\kappa$ for $\lambda_0 = 1550$ nm and the reflectivity for a range of $\Delta\beta$ values between approximately $-7 \times 10^5$ and $8 \times 10^5$ m$^{-1}$.

The fundamental TE mode of a composite waveguide is shown in Figure 1(b). The estimated value of the coupling coefficient for a 100 μm long Bragg grating with a period of $\Lambda = 272$ nm, modulation of $w_1 = 545$ nm and $w_2 = 455$ nm, gain layer thickness of 300 nm, silicon layer thickness of 250 and 50 nm thick $Al_2O_3$ cladding is $\approx$230 cm$^{-1}$. We find the stop band bandwidth to be 8 nm and the two closest reflection minima to be at 1543 and 1554 nm. The confinement factor of the mode inside the gain region for this design is close to 0.5, assuming bulk InGaAsP as a III-V material for computational simplicity. The high achievable confinement factor allows us to build compact lasers through efficient use of the optical mode. The threshold gain is found to be $\approx$150 cm$^{-1}$ for the lowest order longitudinal mode from the resonance condition for a simple DFB laser.[22] This gain value can be achieved in bulk InGaAsP,[23] which is known to exhibit gain coefficients of $\approx$200 cm$^{-1}$ at room temperature.

For experimental demonstration, we choose InGaAsP with multiple quantum wells (MQW) as a gain material. Compared to bulk III-Vs, gain performance can be greatly enhanced in a well optimized III-V MQW structure.[24–26] On the other hand, the optical field confinement factor in the wells is lower than in bulk gain, which would increase the threshold. Comprehensive optimization of these parameters for minimum threshold gain can become rather cumbersome and is outside of the scope of this paper.

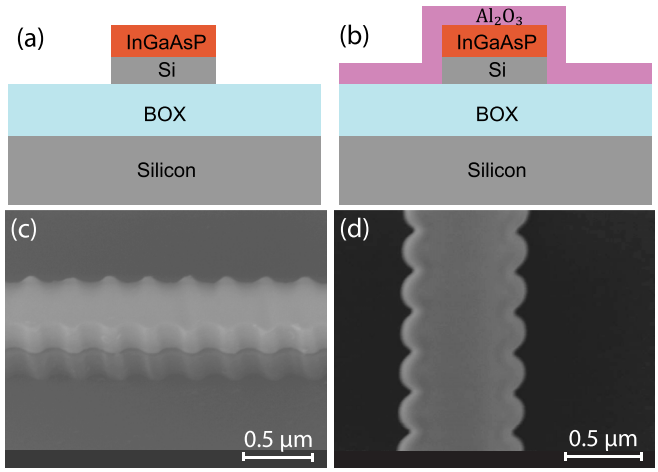


FIG. 2. (a), (b) Schematic steps of fabrication process; (c), (d) the SEM images of the Bragg grating after two-step RIE and after $Al_2O_3$ layer deposition by ALD, respectively.

Composite InGaAsP/Si laser structures were fabricated from an InGaAsP MQW layer bonded to an SOI chip. The schematic drawings of different fabrication steps are shown in Figures 2(a) and 2(b). The MQW InGaAsP/InP wafer was grown by OEpic Semiconductor, Inc. This gain layer is comprised of 9, each 10 nm thick, wells (1.6Q $In_xGa_{1-x}As_yP_{1-y}$, $x = 0.56$, $y = 0.938$ with bandgap wavelength of 1600 nm (1.6Q)) embedded in 10, each 20 nm thick, barriers (1.3Q $In_xGa_{1-x}As_yP_{1-y}$, $x = 0.734$, $y = 0.571$ with bandgap wavelength of 1300 nm (1.3Q)), epitaxially grown on an InP substrate, bringing the total thickness of the gain layer to $\approx$300 nm (the structure is summarized in Table I). This InGaAsP MQW active layer was bonded to an SOI chip with a 250 nm thick top silicon layer via low temperature plasma assisted wafer bonding. This wafer bonding process, as described below, is based on the III-V-to-Si bonding procedure developed by Liang *et al.*[27]

The wafer bonding was performed for a quarter of a 2-in. InGaAsP/InP wafer and a SOI chip of $\approx$10 cm$^2$ area. Prior to the wafer bonding, we etched vertical outgassing channels (VOC) in the top silicon layer of the SOI chip.[27] The purpose of the VOC is to facilitate the evacuation of gaseous byproducts from the InGaAsP/Si interface during the bonding process. We used NR71-1500 PY negative tone photoresist to form the photolithographic mask for the channels. The silicon layer was then etched in a Oxford P100 reactive ion etch (RIE) tool using a $CHF_3$:$SF_6$ chemistry with the following settings: $CHF_3$ and $SF_6$ flows are 15 and 100 sccm, respectively; RIE: 30 W, inductively coupled plasma (ICP): 1200 W, pressure: 15 mTorr, temperature: 20 °C, helium pressure: 10 Torr.

Extremely thorough cleaning procedure of the both wafers is essential for a successful wafer bonding. The low temperature bonding starts with very low power ultrasonication in acetone and isopropanol (IPA), followed by a thorough DI water rinse, to eliminate particles from the bonding

TABLE I. Multiple quantum well InGaAsP/InP epitaxial structure.

| Name | Material | Thickness (Å) | No. layers |
|---|---|---|---|
| Capping layer | InP | 100 | 1 |
| Active region | 1.3Q $In_xGa_{1-x}As_yP_{1-y}$ | 200 | 9 |
| | 1.6Q $In_xGa_{1-x}As_yP_{1-y}$ | 100 | 9 |
| | 1.3Q $In_xGa_{1-x}As_yP_{1-y}$ | 200 | 1 |
| Substrate | InP | 325 μm | |

surfaces and dissolve any remaining organics. Next, the surfaces are to be stripped of native oxides, organic, and ionic contaminations. This is performed on the InGaAsP/InP chip using ammonia hydroxide ($NH_4OH$) for 5 min, and on the $SiO_2$/Si chip using freshly mixed $H_2SO_4$:$H_2O$ (3:1) solution for 5 min. The chemical clean is followed by a quick water gun rinse and drying in $N_2$ flow. Next, both chips are dipped in 1% HF solution for 20 s to remove native oxides. After cleaning, both chips undergo $O_2$ plasma surface activation in a Trion RIE chamber with 20 mTorr pressure, 30 sccm $O_2$ flux, and 50 W RF power for 45 s. The oxygen plasma treatment is immediately followed by a brief rinse in DI water to passivate the active surfaces with hydroxyl (–OH) groups. The water flow also removes any new particles that may have accumulated during the plasma activation. Next, nitrogen flow-dried chips are manually mated. The Van der Waals force between the –OH groups promotes spontaneous mating of activated surfaces. The pair is annealed for 17 h at 300 °C in an oven under atmospheric pressure to form strong covalent bonding and facilitate evacuation of the $H_2O$ and $H_2$ byproducts through the VOC into buried oxide (BOX) layer, and through the BOX away from the InGaAsP/Si interface. Finally, the InP carrier substrate is selectively etched via immersion into 38% HCl at room temperature, until reaction is terminated by the InGaAsP etch stop layer, to obtain the composite InGaAsP/SOI structure.

The next step is to perform the self-aligned etch to create the Bragg grating structures on the bonded chip. This is done through a double step RIE, which has to be carried out on the gain layer and $SiO_2$ using appropriate etching chemistry for each of the two materials. To create the initial mask, E-beam lithographic processing with Raith50 writer is performed on hydrogen silsesquioxane (HSQ) negative resist. This is followed by the two-step RIE to form the top (III-V) layer and bottom (Si) layer of the Bragg grating. First, the 300 nm thick InGaAsP MQW layer is dry etched in $CH_4$:$H_2$:Ar (4:40:20 sccm) chemistry. Then the Si layer undergoes $CHF_3$:$SF_6$ RIE, using the same recipe as for the VOC etching described above, to etch the silicon layer using the gain layer as a mask. Figure 2(a) depicts a schematic drawing of the structure after both of these steps are performed. Next the sample is treated in microwave oxygen plasma (Tepla 100) to eliminate polymer buildup. An SEM image of a clean laser sample after this cleaning step is presented in Figure 2(c). Lastly, atomic layer deposition (ALD) of 50 nm thick $Al_2O_3$ is carried out using a Beneq TFS200 for thermal management (Figure 2(b) shows a diagram of the resultant structure). An SEM image of the Bragg grating after the aluminum oxide deposition is shown in Figure 2(d).

We used a standard micro-photoluminescence setup for optical characterization of the lasers. For optical pumping, we employed a 1064 nm pulsed fiber laser (SPI G3) with a repetition rate of 300 kHz and 12 ns pulse width. The pump beam was focused down to an approximately 20 × 570 $\mu m^2$ spot size (FWHM) at the sample plane, using a combination of cylindrical and spherical lenses. This spot size calculation includes the effect of the pump beam's quality factor ($M^2$) of 1.84 (provided by the laser manufacturer). The edge of the sample was imaged onto an infrared (IR) InGaAs camera (Indigo Alpha NIR) through a 20× IR-coated microscope objective and a double 4–f imaging system. The output signal was collected through the same objective and passed through a pump filter (1064 nm Semrock RazorEdge longpass), onto either the IR camera or a monochromator (Spectral Products DK480). Both total power measurements for the light-light curves and high resolution measurements in the lasing operation mode were performed with the monochromator, which has a resolution of 0.35 nm and is equipped with a cooled InGaAs detector in lock-in detection configuration. All measurements were performed at room temperature.

The optical measurements results for the DFB laser with design physical dimensions are shown in Figures 3 and 4. The actual structure may slightly differ from the design due to fabrication inaccuracies. The plot in Figure 3 represents spectral evolution from a broad-band photoluminescence at lower pump powers through amplified spontaneous emission (ASE) to a single narrow peak at 1515 nm wavelength, as the power increases. The width of the peak at the highest pump powers was limited by the monochromator resolution of 0.35 nm. We observed appearance of coherence rings around the output mode on the IR camera (Figure 4, upper left inset), which is one of the signatures of stimulated emission. We measured the extinction ratio between the TE-like and TM-like modes to be higher than 20 dB.

To extract the lasing threshold, we performed light-light measurements (Figure 4) and analyzed the corresponding logarithmic scale plot (Figure 4, lower right inset). The S-shaped log-log curve is characteristic of laser behavior. In the ideal

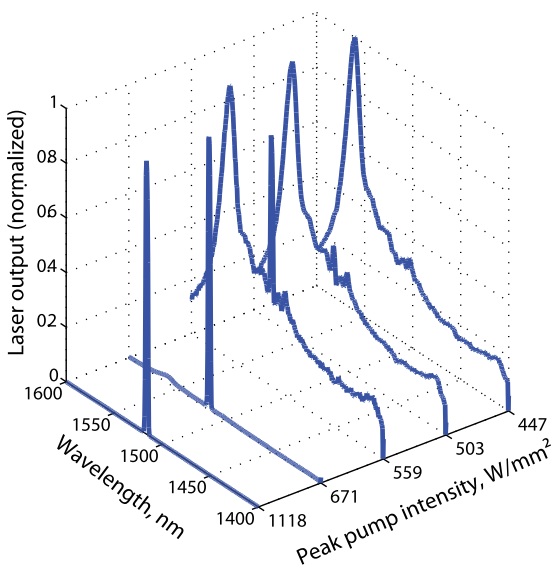


FIG. 3. Spectral evolution, with final peak wavelength at 1515 nm.

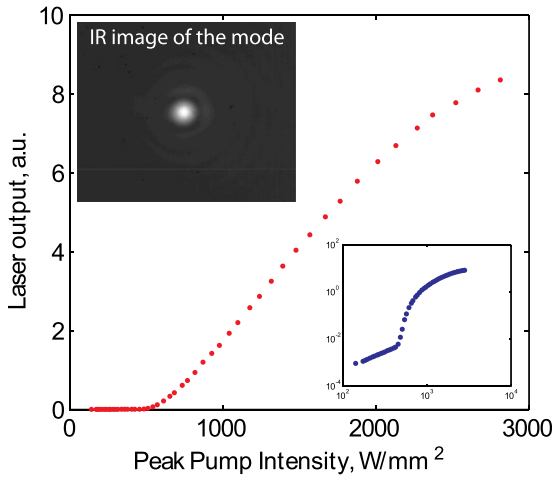


FIG. 4. The laser light-light curve in linear and logarithmic (lower right inset) scale with the IR image (upper left inset) of the lasing mode; lasing threshold is at 530 W/mm$^2$.

case (when the recombination only occurs through radiative excitonic transitions), the first and last sections of the curve are linear with slopes close to 1. We found the threshold peak pump intensity to be around 530 W/mm$^2$, assuming lasing threshold to be at the middle point of the ASE section. For the III-V/Si DFB laser, the PL and stimulated emission sections exhibit varying slope, which deviates from unity. The superlinear behavior of the light-light characteristic in these regions points to various cavity and material losses, including scattering losses, surface recombination, and non-radiative recombination on the III-V/Si interface. This is a fairly common for a realistic nanoscale structure,[28,29] due to the high density of defects per volume.

To summarize the results, we demonstrated a compact optically pumped III-V/Si DFB laser with sidewall modulated Bragg gratings. The laser structure is 100 μm long with average waveguide width of 500 nm and a total waveguide height of 550 nm. We employed plasma-assisted wafer bonding and a self-aligned fabrication approach in making the laser, a process that does not require any lithographic alignment with its associated alignment losses. The flexibility of a sidewall modulated grating design can also enable the development of low-threshold hybrid DFB lasers, with larger physical size. Work on an electrically pumped version of the laser, as well as coupling of the lasing mode to a silicon waveguide, is underway.

This work was supported by the Defense Advanced Research Projects Agency (DARPA), the National Science Foundation through CIAN NSF ERC under grant #EEC-0812072, the Oracle Labs, the Cymer Corporation, and the U.S. Army Research Office. The fabrication was performed at UCSD Nano3 facilities. The authors would like to thank Felipe Vallini, Michael Kats and Maziar Nezhad for helpful discussions.

[1]D. A. B. Miller, IEEE J. Sel. Topics Quantum Electron. **6**, 1312 (2000).
[2]B. Jalali and S. Fathpour, J. Lightwave Technol. **24**, 4600 (2006).
[3]N. Izhaky, M. T. Morse, S. Koehl, O. Cohen, D. Rubin, A. Barkai, G. Sarid, R. Cohen, and M. J. Paniccia, IEEE J. Sel. Topics Quantum Electron. **12**, 1688 (2006).
[4]J. M. Fedeli, R. Orobtchouk, C. Seassal, and L. Vivien, Proc. SPIE **6125**, 61250H (2006).
[5]K. Ohira, K. Kobayashi, N. Iizuka, H. Yoshida, M. Ezaki, H. Uemura, A. Kojima, K. Nakamura, H. Furuyama, and H. Shibata, Opt. Express **18**, 15440 (2010).
[6]T. Aalto, M. Harjanne, M. Kapulainen, S. Ylinen, and L. Mörl, Proc. SPIE **7943**, 79430V (2011).
[7]J. E. Cunningham, A. V. Krishnamoorthy, R. Ho, I. Shubin, H. Thacker, J. Lexau, D. C. Lee, D. Feng, E. Chow, Y. Luo, X. Zheng, G. Li, J. Yao, T. Pinguet, K. Raj, M. Asghari, and J. G. Mitchell, IEEE J. Sel. Topics Quantum Electron. **17**, 546 (2011).
[8]R. Chen, T.-T. D. Tran, K. W. Ng, W. S. Ko, L. C. Chuang, F. G. Sedgwick, and C. Chang-Hasnain, Nature Photon. **5**, 170 (2011).
[9]C.-W. Hsu, Y.-F. Chen, and Y.-K. Su, IEEE Photon. Technol. Lett. **24**, 1009 (2012).
[10]C. Hahn, Z. Zhang, A. Fu, C. H. Wu, Y. J. Hwang, D. J. Gargas, and P. Yang, ACS Nano **5**, 3970 (2011).
[11]S. Lourdudoss, Curr. Opin. Solid State Mater. Sci. **16**, 91 (2012).
[12]F. Niklaus, R. J. Kumar, J. J. McMahon, J. Yu, J. Q. Lu, T. S. Cale, and R. J. Gutmann, J. Electrochem. Soc. **153**, G291 (2006).
[13]D. Liang, A. W. Fang, H. Park, T. E. Reynolds, K. Warner, D. C. Oakley, and J. E. J. Electron. Mater. **37**, 1552 (2008).
[14]M. J. R. Heck, J. Bauters, M. Davenport, J. Doylend, S. Jain, G. Kurczveil, S. Srinivasan, Y. Tang, and J. E. Bowers, IEEE J. Sel. Topics Quantum Electron. **19**, 6100117 (2013).
[15]D. Liang, M. Fiorentino, T. Okumura, H.-H. Chang, D. T. Spencer, Y.-H. Kuo, A. W. Fang, D. Dai, R. G. Beausoleil, and J. E. Bowers, Opt. Express **17**, 20355 (2009).
[16]H.-C. Kim, K. Ikeda, and Y. Fainman, Opt. Lett. **32**, 539 (2007).
[17]H. Park, A. Fang, O. Cohen, R. Jones, M. Paniccia, and J. Bowers, IEEE J. Sel. Topics Quantum Electron. **12**, 1657 (2006).
[18]S. Srinivasan, A. W. Fang, D. Liang, J. Peters, B. Kaye, and J. E. Bowers, Opt. Express **19**, 9255 (2011).
[19]S. Stanković, R. Jones, M. Sysak, J. Heck, G. Roelkens, and D. Van Thourhout, IEEE Photon. Technol. Lett. **24**, 2155 (2012).
[20]H. Kogelnik and C. Shank, J. Appl. Phys. **43**, 2327 (1972).
[21]P. Y. A. Yariv, *Optical Waves in Crystals: Propagation and Control of Laser Radiation* (John Wiley and Sons, Hoboken, NJ, 2003), pp. 194–201, 560–575.
[22]G. Morthier and P. Vankwikelberg, *Handbook of Distributed Feedback Laser Diodes* (Artech House, Inc., Norwood, MA, 1997), pp. 93–121.
[23]E. O. Goebel, G. Luz, and E. Schlosser, IEEE J. Quantum Electron. **15**, 697 (1979).
[24]L. Coldren and S. Corzine, *Diode Lasers and Photonic Integrated Circuits* (John Wiley and Sons, New York, NY, 1995).
[25]J. Shimizu, H. Yamada, S. Murata, A. Tomita, M. Kitamura, and A. Suzuki, IEEE Photon. Technol. Lett. **3**, 773 (1991).
[26]M. Korbl, A. Groning, H. Schweizer, and J. L. Gentner, J. Appl. Phys. **92**(5), 2942 (2002).
[27]D. Liang, J. E. Bowers, D. C. Oakley, A. Napoleone, D. C. Chapman, L. C. Chen, P. W. Juodawlkis, and O. Raday, Electrochem. Solid-State Lett. **12**, H101 (2009).
[28]O. Bondarenko, A. Simic, Q. Gu, J. H. Lee, B. Slutsky, M. P. Nezhad, and Y. Fainman, IEEE Photon. J. **3**, 608 (2011).
[29]K. Srinivasan, M. Borselli, O. Painter, A. Stintz, and S. Krishna, Opt. Express **14**, 1094 (2006).